JOURNAL OF COMPUTATIONAL PHYSICS 115, 431–439 (1994)

A Singularities Tracking Conservation Laws Scheme for Compressible Duct Flows

J. FALCOVITZ

Department of Aerospace Engineering, Technion, Haifa 32000, Israel

AND

A. BIRMAN

Department of Physics, Technion, Haifa 32000, Israel

Received September 7, 1993; revised May 27, 1994

A singularities tracking version of the GRP scheme for the integration of the Euler equations for compressible duct flow is presented. Flow singularities corresponding to contact (material), shock, or gradient discontinuities are represented by special grid points that move through the fixed grid at the appropriate speed of propagation. The primary modification to the Eulerian GRP scheme is the evaluation of fluxes at singular points in a unified grid containing the union of regular Euler grid points and singular moving points. Interactions between singular points (shock–shock or shock–contact interactions) are treated accurately by solving the appropriate generalized Riemann problem. The new GRP/ST scheme combines some merits of computation by characteristics, with a robustness approaching that of a finite difference conservation laws scheme. Shock wave phenomena illustrating the capabilities of the tracking method are presented, demonstrating improved resolution and accuracy at a given grid.

I. INTRODUCTION

The one-dimensional Euler equations that govern the adiabatic time-dependent flow of an inviscid fluid in a duct of varying cross section admit solutions that may contain hydrodynamic discontinuities of three types: a shock discontinuity, a contact discontinuity, and a discontinuity in spatial gradients of flow variables. The only exact method for computing solutions to these equations is the method of characteristics (MOC), where the solution is constructed by integrating the differential relations that hold along characteristic lines in (x, t). When hydrodynamic singularities are present in the flow, the MOC construction is augmented by jump conditions that hold at shock or contact discontinuities; at a gradient discontinuity the flow variables are continuous, and it propagates along a characteristic line. The sole factor hindering the practical application of the MOC is its excessive complexity.

It is against this background that the alternate approach of conservation laws schemes has been extensively pursued and has evolved into a genre of shock-capturing higher order schemes based on solutions to Riemann problems at cell interfaces (e.g., [1, 2, 14]); see also [16] for an overview of existing methods. Although the resolution achieved by these schemes is remarkable, it is still unsatisfactory in problems involving a combination of high gradients and shock interactions. In this study we present a "singularities tracking" extension to the high-resolution conservation laws scheme GRP [1, 2], designed to render accurate computation through tracking of hydrodynamic singularities as well as those resulting from their interactions. A preliminary account of our method was presented in [5] and a more comprehensive report in [6]. We precede the description of the tracking scheme by a brief outline of the GRP method [1, 2].

The GRP discretisation scheme is a piecewise-linear approximation of primitive flow variables (velocity, pressure, density) per cell, with discontinuities at cell interfaces. There is an inherent duality in this scheme, in that both cell-interface and cell-average values of flow variables are evaluated in the course of integrating the hydrodynamic conservation laws, performed in three phases as follows. In the first phase, cell-interface values are obtained from a local MOC analysis yielding an analytic solution to the generalized Riemann problem arising at each cell interface. This is followed by evaluating the fluxes of mass, momentum, and energy at cell interfaces; in particular, second-order accurate fluxes are evaluated from analytically determined fluxes and their first time derivatives. In the second phase, the fluxes are incorporated in a discrete time-integration scheme for the average densities of mass, momentum, and energy per cell. In the third phase, cell gradients of primitive variables are advanced to the next time level, using the time derivatives at cell interfaces (obtained in the first phase), and subject to monotonicity-preserving constraints [1, 2, 14]. The combined result is a second-order accurate integration of the hydrodynamic conservation laws.

0021-9991/94 $6.00

Our GRP/ST "singularities tracking" scheme is designed to exploit the cell-interface solutions to generalized Riemann problems performed in phase I of the GRP scheme. To this effect we assign a special (moving) grid point to each tracked discontinuity. The resulting "unified grid" comprises a union of the underlying Eulerian grid and all moving "singularity points." The analytic GRP solution at each unified grid point provides both the velocity and the acceleration of every shock, contact, or gradient discontinuity arising in the solution to the associated Riemann problem [1, 2]; thus, selection of the appropriate wave at a tracked singularity point enables a straightforward second-order time integration of its trajectory. In order to avoid formation of excessively small cells in the unified grid, a Eulerian grid point located within a fraction β of cell size from a moving singularity point is temporarily deleted (typically, $\beta = 0.25$). The deletion (resp., restoration) of Eulerian grid points is performed as a cell-merging (resp., cell-splitting) operation, conserving total mass, momentum, and energy.

The tracking of waves resulting from local Riemann problems has been formerly suggested by Harten and Hyman [7] as a "self-adjusting" grid scheme for the Godunov method. However, their extended "weighted-average" wave tracking concept does not universally reduce to explicit tracking of a single wave (compare, e.g., Figs. 6, 10 in [7]). The feature of combining exact shock tracking with a conservation laws scheme was also adopted by Swartz and Wendroff [11] and in a recent study by LeVeque and Shyue [8], where a concise discussion of previous work on shock fitting and shock tracking was presented. Our scheme, however, is different from those schemes in three important aspects. First and foremost is the way second-order accuracy is obtained; second is the treatment of duct flows; third is the manner by which excessively small partial cells adjacent to tracked singularity points are avoided.

The major feature unique to our scheme is the systematic method by which we obtain second-order accuracy for planar flows, as well as for duct flows. In the GRP/ST scheme, second-order accuracy is obtained from analytically evaluated first time derivatives of flow variables; in particular, this includes first time derivatives of the velocity of propagation of tracked singularity points. Under this unified analytic approach, generalized Riemann problems include terms related to both linear spatial interpolation of flow variables and to area divergence in a duct flow. The other two shock-tracking schemes referred to above comprise a first-order phase where conservation laws are integrated using solutions to local Riemann problems, followed by a separate phase for upgrading the accuracy level to second order. In addition, LeVeque and Shyue [8] treat area divergence terms in a duct flow as source terms in the planar conservation laws.

When singularity points are tracked on a grid in conjunction with the discrete integration of conservation laws, formation of small partial cells is inevitable. While our GRP/ST scheme circumvents this difficulty by cell-merging/cell-splitting, Le Veque and Shyue [8] resort to a large time step alternative, where, in the vicinity of a tracked point, the discretised conservation laws are integrated via a wave propagation approach rather than a conservation laws scheme. Swartz and Wendroff [11] treat the integration of conservation laws in the vicinity of a shock point, by resorting to substepping of the time integration, in order to avoid an overall reduction of the time step. Unlike the modified time integration employed by [8, 11], our scheme comprises a simple time-integration by a uniform time step; formation of excessively small cells is avoided by cell splitting/merging as outlined above.

The initiation of shock tracking in our scheme may be in either of two modes. In mode I the shock is known to exist from the initial conditions of the problem, and is tracked from the beginning of the computation. In mode II, the "trapping" mode, shock-tracking is initiated at some Eulerian grid point, when the solution to the local Riemann problem indicates the inception of a shock of substantial intensity. Mode I also encompasses the case where a new shock is created by a shock interaction (e.g., shock-contact interaction giving rise to two shocks).

The plan of this paper is the following. The conservation laws and the finite-difference scheme are presented in Section 2, supplemented by the analytic derivation of time derivatives along the shock path in Section 3. We conclude with five examples demonstrating the capabilities of the GRP/ST scheme in Section 4.

2. CONSERVATION LAWS IN A MOVING GRID

Consider the Euler equations governing the time-dependent flow of an inviscid fluid in one space dimension x and in a duct of smoothly varying cross-section $A(x)$. In quasi-conservation form, these equations are

$$A\frac{\partial}{\partial t}U + \frac{\partial}{\partial x}[A\mathbf{F}(\mathbf{U})] + A\frac{\partial}{\partial x}[\mathbf{G}(\mathbf{U})] = 0$$

$$\mathbf{U}(x,t) = \begin{bmatrix} \rho \\ \rho u \\ \rho E \end{bmatrix} \quad \mathbf{F}(\mathbf{U}) = \begin{bmatrix} \rho u \\ \rho u^2 \\ (\rho E + p)u \end{bmatrix} \quad \mathbf{G}(\mathbf{U}) = \begin{bmatrix} 0 \\ p \\ 0 \end{bmatrix} \tag{2.1}$$

$$E = e + \tfrac{1}{2}u^2 \quad p = f(\rho, e) \quad A = A(x),$$

where ρ, p, e, u, E are the density, pressure, specific energy, velocity, and total energy, respectively; in addition, an equation of state $p = f(\rho, e)$ is assumed.

Aiming at a finite-difference scheme for (2.1) in a mixed-type grid where some grid points may be moving (see also [3, 4]), let us consider a moving zone $D_t = \{x | a(t) \leq x \leq b(t)\}$.

Assuming that the flow in D_t is smooth, we get the integral relation

$$\frac{d}{dt}\int_{D_t} A(x)\mathbf{U}(x,t)\,dx = \int_{D_t} A(x)\frac{\partial}{\partial t}\mathbf{U}(x,t)\,dx + b'(t)A(b(t))\mathbf{U}(b(t),t) - a'(t)A(a(t))\mathbf{U}(a(t),t). \tag{2.2}$$

Using this relation in Eq. (2.1) for $(\partial U/\partial t)$, we get the quasi-conservation relation

$$\frac{d}{dt}\int_{D_t} A\mathbf{U}\,dx = [(\Lambda\mathbf{U} - \mathbf{F}(\mathbf{U}))A]_{a(t),t}^{b(t),t} - \int_{D_t} A(x)\frac{\partial}{\partial x}\mathbf{G}(\mathbf{U})\,dx \tag{2.3}$$

where $\Lambda(a(t), t) = a'(t)$ and $\Lambda(b(t), t) = b'(t)$.

Having ruled out the existence of a hydrodynamic discontinuity (shock or contact) in the interior of D_t, we consider the existence of a discontinuity at either boundary of D_t. The appropriate boundary values $\mathbf{U}(a(t), t)$, or $\mathbf{U}(b(t), t)$ in (2.3), are clearly the "inner side" values; i.e., the right-side values at $a(t)$ and the left-side values at $b(t)$. Actually, this side distinction is immaterial for the mass and energy equations since they are in conservation form, and according to the jump condition obeyed by hydrodynamic discontinuities, the jump in the value of $[\Lambda\mathbf{U} - \mathbf{F}(\mathbf{U})]$ vanishes. The momentum equation, however, is in non-conservation form, so for this equation side distinction is essential.

The finite-difference scheme for the integration of (2.1) is obtained by dividing the spatial domain into cells $i = 1, 2, \ldots, i, \ldots, I$, where cell boundaries are the points $x_{1/2}, x_{3/2}, \ldots, x_{i-1/2}, x_{i+1/2}, \ldots, x_{I+1/2}$. The time integration is at a sequence of time points $t_n = n\,\Delta t$, where the magnitude of Δt is constrained by the Courant–Friedrichs–Levy stability criterion. We denote by $\mathbf{U}_i^n$ the volume average of $\mathbf{U}(x, t)$ in cell i at time t_n; $x_{i+1/2}^n$ denotes the coordinate of grid point $i + 1/2$ at time t_n. Taking the domain D_t to be cell i with possibly moving grid points at either end, the finite-difference scheme based on (2.3) is

$$\mathbf{U}_i^{n+1} = \frac{V_i^n}{V_i^{n+1}}\mathbf{U}_i^n + \frac{\Delta t}{V_i^{n+1}}\{[(\Lambda\mathbf{U} - \mathbf{F}(\mathbf{U}))A]_{i+1/2}^{n+1/2} - [(\Lambda\mathbf{U} - \mathbf{F}(\mathbf{U}))A]_{i-1/2}^{n+1/2} - \frac{1}{2}[\mathbf{G}(\mathbf{U})_{i+1/2}^{n+1/2} - \mathbf{G}(\mathbf{U})_{i-1/2}^{n+1/2}](A_{i+1/2}^{n+1/2} + A_{i-1/2}^{n+1/2})\}, \tag{2.4}$$

where $A_{i+1/2}^{n+1} = A(x_{i+1/2}^{n+1/2})$ and the cell volume V_i^n is given by

$$V_i^n = \int_{x_{i-1/2}^n}^{x_{i+1/2}^n} A(x)\,dx. \tag{2.5}$$

In addition, the new coordinate of a moving grid point is given by

$$x_{i+1/2}^{n+1} = x_{i+1/2}^n + \Lambda_{i+1/2}^n\,\Delta t + \frac{1}{2}\left[\frac{d\Lambda}{dt}\right]_{i+1/2}^n(\Delta t)^2. \tag{2.6}$$

As in the original duct-flow GRP [2], the time-centered flux is obtained by

$$[(\Lambda\mathbf{U} - \mathbf{F}(\mathbf{U}))A]_{i+1/2}^{n+1/2} = [(\Lambda\mathbf{U} - \mathbf{F}(\mathbf{U}))A]_{i+1/2}^n + \frac{1}{2}\Delta t\frac{d}{dt}[(\Lambda\mathbf{U} - \mathbf{F}(\mathbf{U}))A]_{i+1/2}^n \tag{2.7}$$

$$[\mathbf{G}(\mathbf{U})]_{i+1/2}^{n+1/2} = [\mathbf{G}(\mathbf{U})]_{i+1/2}^n + \frac{1}{2}\Delta t\frac{d}{dt}[\mathbf{G}(\mathbf{U})]_{i+1/2}^n,$$

where (d/dt) denotes the time derivative along the path of a moving grid point. In evaluating this derivative, $\mathbf{U}$, $\mathbf{F}(\mathbf{U})$, and $\mathbf{G}(\mathbf{U})$ are expressed in terms of the primitive variables p, ρ and u, so that (2.7) calls for the evaluation of the derivatives of these primitive variables along the path of the grid point; in addition, the time derivatives $[(d/dt)\,\Lambda]_{i+1/2}^n$ is also required.

Consider first the time derivatives of the primitive variables, whose evaluation constitutes an extension of the Eulerian GRP to a scheme on a mixed grid of stationary or moving points (see Sec. 5 of Ref. [2]). We seek the time derivative of $Q(\xi, t)$, where Q stands for p, ρ, or u, ξ is the Lagrange coordinate defined by $d\xi = A_{i+1/2}^n\rho dx$, and the path of grid point $i + 1/2$ is given by the differential relation

$$\frac{d\xi}{dt} = -[A\rho(u - \Lambda)]_{i+1/2}^n. \tag{2.8}$$

The derivation of (2.8) is readily obtained by considering the relation for the moving coordinate $x = x(\xi, t)$: $dx = (\partial x/\partial\xi)\,d\xi + (\partial x/\partial t)\,dt = \Lambda\,dt$; Equation (2.8) then follows by substituting $(\partial x/\partial\xi) = (A\rho)^{-1}$ and $(\partial x/\partial t) = u$. Using the chain rule

$$\frac{d}{dt}Q(\xi(t), t) = \left(\frac{\partial}{\partial t} + \frac{d\xi}{dt}\frac{\partial}{\partial\xi}\right)Q(\xi, t)$$

we get

$$\left[\frac{dQ}{dt}\right]_{t=0} = \left[\frac{\partial}{\partial t}Q(\xi, t)\right]_{t=0} - \left[A\rho(u - \Lambda)\frac{\partial}{\partial\xi}Q(\xi, t)\right]_{t=0}, \tag{2.9}$$

where $(\xi, t) = (0, 0)$ denotes the origin of the local (ξ, t) coordinates at $(x_{i+1/2}^n, t_n)$. Clearly, (2.9) reverts to the Eulerian GRP when $\Lambda = 0$ (see Eq. (5.3) in [2]).

Now, in our scheme a moving grid point is either a contact discontinuity or a shock discontinuity. For a contact discontinuity $\Lambda = u$, hence in this case the second term of (2.9) vanishes and $(dQ/dt)_{t=0}$ becomes the time derivative along the contact

discontinuity; this time derivative constitutes the basic analytic outcome of the local generalized Riemann problem at each grid point. Hence, the case of a contact discontinuity is already contained in the analytic framework of the existing GRP scheme [2, 4]. The case of a shock discontinuity, by contrast, requires further analysis and is relegated to the next section.

3. TIME DERIVATIVES ALONG A SHOCK PATH

To fix ideas, let us consider a typical generalized Riemann problem where the wave system comprises a right shock and a left rarefaction. The coordinates, as before, are (ξ, t) with the origin located at $(x^n_{i+1/2}, t_n)$. Let the suffix $(\,)_*$ refer to the (ξ, t) region between the contact discontinuity and the shock, and let $(\,)_r$ refer to the region ahead (to the right) of the shock. Also, the cross-section area $A(x^n_{i+1/2})$ is simply denoted by A.

In the course of the analysis, ξ-derivatives in region $(\,)_*$ are expressed in terms of time derivatives and, likewise, time derivatives in region $(\,)_r$ are expressed in terms of ξ-derivatives. The reason is that in the GRP scheme primitive variables are approximated as piecewise-linear per cell; i.e., $Q(\xi, 0)$ is linear, so that Q_r and its ξ-derivative are known; the solution to the generalized Riemann problem then provides the time derivatives $[(\partial/\partial t)\, Q(\xi, t)]_{t=0}$ in region $(\,)_*$. For this derivatives-swapping operation, use is made of the governing equations in Lagrange coordinate

$$\begin{aligned} \frac{\partial}{\partial t} u(\xi, t) &= -A \frac{\partial}{\partial \xi} p(\xi, t) \\ \frac{\partial}{\partial t} \tau(\xi, t) &= A \frac{\partial}{\partial \xi} u(\xi, t) + \lambda \tau u \\ \lambda &= A'(x)/A(x) \qquad \tau = 1/\rho, \end{aligned} \tag{3.1}$$

where τ is the specific volume and λ is the logarithmic derivative of the local cross-section area.

Let the Lagrange speed of propagation of the shock be $d\xi/dt = W$. Since $d\xi = A\rho dx$, the relation between W and the Eulerian speed Λ is

$$\Lambda = u_r + \tau_r (A^{-1}W). \tag{3.2}$$

The expression for the time derivative of Λ is obtained by Lemmas 3.1 and 3.2, as follows.

LEMMA 3.1. *Assume the typical wave system as before. Then*

$$\begin{aligned} \frac{d\Lambda}{dt} = &- A \left(\frac{\partial p}{\partial \xi}\right)_r + 2W \left(\frac{\partial u}{\partial \xi}\right)_r + A(A^{-1}W)^2 \left(\frac{\partial \tau}{\partial \xi}\right)_r \\ &+ \lambda W u_r \tau_r + \tau_r \frac{d}{dt}(A^{-1}W). \end{aligned} \tag{3.3}$$

Proof. To derive (3.3) we use the chain rule $(d/dt) = ((\partial/\partial t) + W(\partial/\partial \xi))$ for the time derivative along the shock, applying it to the right-hand side of Eq. (3.2), while taking u_r and τ_r to be functions of (ξ, t). Using (3.1) to express time derivatives of $u(\xi, t)$ and $\tau(\xi, t)$ in terms of ξ-derivatives, we get (3.3). Q.E.D.

To proceed, we have to relate the time derivative of $(A^{-1}W)$ appearing in (3.3) to the flow variables. For this, we make use of the following expression for the Lagrange shock speed

$$W = A \frac{p^* - p_r}{u_* - u_r}. \tag{3.4}$$

The time derivative of $A^{-1}W$ is then given by the following lemma.

LEMMA 3.2. *Assume the typical wave system as before. Then*

$$\begin{aligned} \frac{d}{dt}(A^{-1}W) = \frac{1}{(u_* - u_r)} \Bigg\{ &\left[1 + \frac{(A^{-1}W)^2}{g_*^2}\right] \left(\frac{\partial p}{\partial t}\right)_* \\ &- 2(A^{-1}W) \left(\frac{\partial u}{\partial t}\right)_* - 2W \left(\frac{\partial p}{\partial \xi}\right)_r \\ &+ A[(A^{-1}W)^2 + g_r^2] \left(\frac{\partial u}{\partial \xi}\right)_r \\ &+ \lambda [(A^{-1}W)^2 u_* \tau_* + g_r^2 u_r \tau_r] \Bigg\}, \end{aligned} \tag{3.5}$$

where $g^2 = -(\partial p/\partial \tau)_s$.

Proof. The derivation of (3.5) starts by applying $(d/dt) = ((\partial/\partial t) + W(\partial/\partial \xi))$ to $(A^{-1}W)$ as given by (3.4), getting an expression that contains both time- and ξ-derivatives of p and u at $(\,)_*$ and at $(\,)_r$. Using (3.1) to express the time derivatives at $(\,)_r$ in terms of ξ-derivatives, and likewise the ξ-derivatives at $(\,)_*$ in terms of time derivatives, and rearranging terms, we get (3.5). Q.E.D.

Combining Lemmas 3.1 and 3.2, we have completed the expression of $(d/dt)\,\Lambda$ in terms of known values of primitive variables and their derivatives.

One more analytic derivation is called for in the case of a very weak shock, i.e., a sound wave. In this case, we simply set $(A^{-1}W) = g_r = g_*$; (3.4) then reduces to the differential relation $g = (dp/du)$. Carrying out the derivation for a perfect gas having a specific heats ratio γ, we get

$$\begin{aligned} \frac{d\Lambda}{dt} = &\left(\frac{3-\gamma}{2}\right) g_r A \left(\frac{\partial u}{\partial \xi}\right)_r - \left(\frac{2-\gamma}{2}\right) A \left(\frac{\partial p}{\partial \xi}\right)_r \\ &- \frac{1}{2} c_r^2 A \left(\frac{\partial \rho}{\partial \xi}\right)_r - \lambda \left(\frac{\gamma - 1}{2}\right) u_r c_r. \end{aligned} \tag{3.6}$$

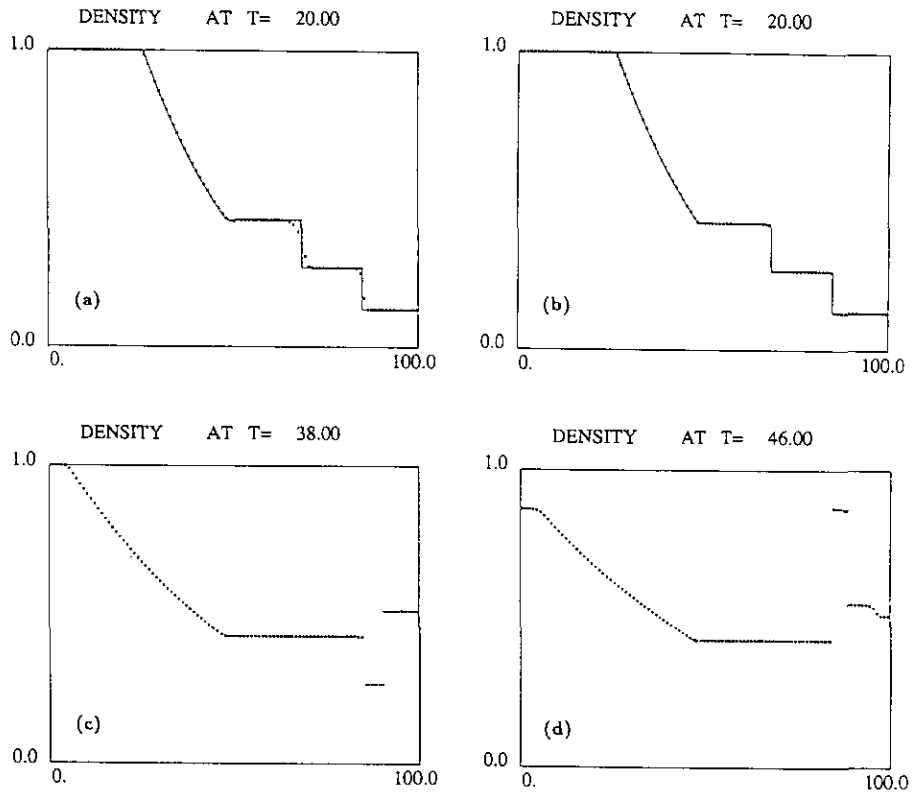

FIG. 1. Sod's problem: (a) at $t = 20$ without tracking of singularities; (b) at $t = 20$ with tracking of the tail of the left-propagating rarefaction, the contact discontinuity, and the right-propagating shock wave; (c) at $t = 38$ with tracking; (d) at $t = 46$ with tracking.

4. SAMPLE PROBLEMS

In this section we present five examples illustrating the scope and accuracy of our scheme, including tracking of shock, contact and gradient discontinuities, post-interaction tracking, and "shock-trapping", i.e., tracking commencing at the inception of a shock formed by the steepening of a smooth compression wave. In each case we track solely those singularities that are deemed most significant.

As demonstrated below, the GRP/ST scheme yields high-resolution computations of complex 1-D compressible flow phenomena involving shock propagation and shock interactions, with a large improvement in accuracy and resolution relative to shock-capturing conservation-laws schemes (e.g., the Eulerian GRP). It is noted that in GRP/ST improved accuracy and resolution are achieved at a modest increase in computing time and coding effort relative to shock-capturing schemes.

(a) *Planar Shock Tube*

Our first example is the planar shock-tube test problem suggested by Sod [10]. The tube extends from $x = 0$ to $x = 100$ and is divided into 100 equal Eulerian cells. The gas ($\gamma = 1.4$) is initially at rest with $p = \rho = 1$ for $0 \leq x < 50$; $p = 0.1$, $\rho = 0.125$ for $50 < x \leq 100$. We show the density profile at $t = 20$ for two computations. The first one, Fig. 1a, with no singularity tracking (pure Eulerian), and the second one, Fig. 1b, with tracking of the tail characteristic of the left-propagating rarefaction wave, the contact discontinuity, and the shock wave. The GRP/ST computation almost coincides with the exact (self-similar) solution.

Shock interactions in GRP/ST are shown in Figs. 1c and 1d, where we show the density profile at two later points in time. At $t = 38$ (Fig. 1c), the shock has been reflected from the right wall but has not yet reached the contact discontinuity. At $t = 46$ (Fig. 1d), the shock has interacted with the contact discontinuity, producing a left-propagating shock, a contact discontinuity, and a right-propagating shock, of which only the first two are tracked, since the right-propagating shock is rather weak.

(b) *Exploding Helium Sphere*

This example, which is a spherical shock tube, was suggested by Saito and Glass [9]. A helium ($\gamma = 5/3$) sphere of radius 2.5 is surrounded by air ($\gamma = 7/5$) and is initially at rest with

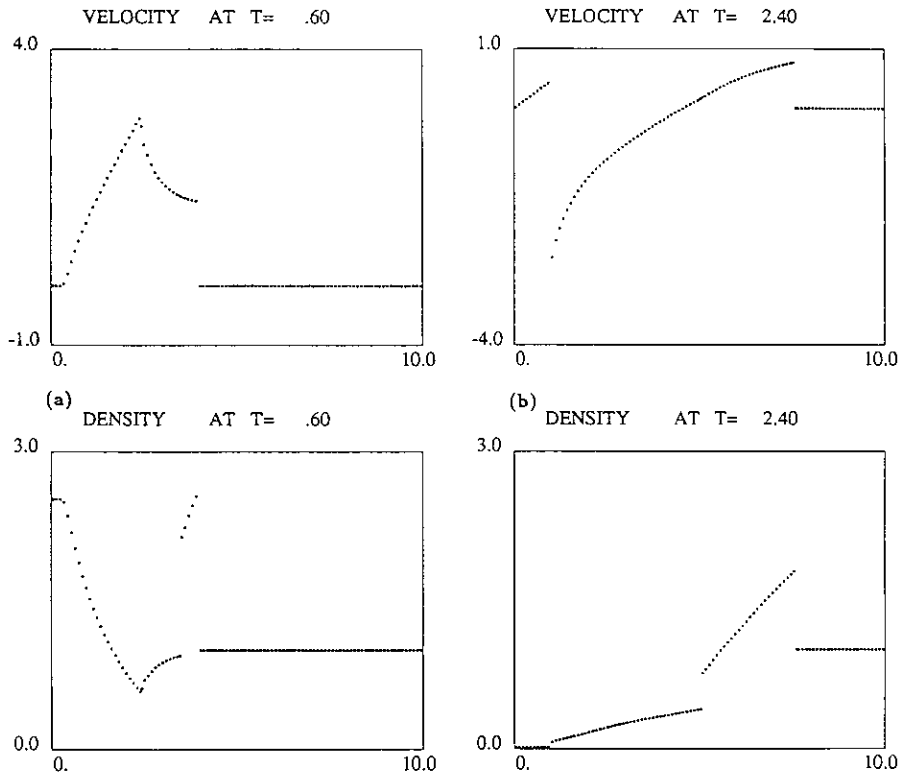

FIG. 2. Exploding helium sphere: (a) at $t = 0.6$ with tracking of the tail of the left-propagating rarefaction, the contact discontinuity, and the right-propagating shock wave; (b) at $t = 2.4$ with tracking of the left imploding shock, the contact discontinuity, and the right-propagating shock wave.

a pressure 18.25 times the air pressure, and a uniform density 2.523 times that of the air. The flow is considered at two instances: (a) At $t = 0.60$, after the initial discontinuity has been resolved into a left-propagating rarefaction wave, of which we tracked the tail, and a contact discontinuity and a right-propagating shock, both of which were tracked (see Fig. 2a). (The tracked tail of the rarefaction wave is the cusp point at both the velocity and density profiles.) (b) At $t = 2.40$, long after the rarefaction wave has been reflected from the center of the sphere and was overtaken by an imploding shock (see Fig. 2b). The resolution in both figures is far superior to that of a previous computation where only the contact discontinuity was tracked [4]. An interesting mode of shock computation is demonstrated in this case. The imploding shock formed as a result of the overexpansion of the helium sphere (and computed as a captured shock), overtook the left-propagating sound wave, which had initially been designated to track the tail of the helium rarefaction wave; from that moment on, the computation of the tracked sound wave reverted to that of a tracked shock. This imploding shock is clearly visible on Fig. 2b at about $x = 1$.

(c) *Interacting Blast Waves*

This test problem was introduced by Woodward and Colella [15], who analyzed it in great detail; it involves multiple asymmetric interactions of strong blast waves. The fluid is a perfect gas ($\gamma = 1.4$) initially at rest ($u_0 = 0$) between reflecting walls in the domain $0 < x < 1$, and has uniform density ($\rho_0 = 1$). The initial pressure is piecewise constant in three zones as follows: in the left zone ($0 < x < 0.1$) the pressure is $p_0 = 1000$, in the middle zone ($0.1 < x < 0.9$) the pressure is $p_0 = 0.01$, and in the right zone ($0.9 < x < 1$) it is $p_0 = 100$. In the GRP/ST computation, the mesh size was a uniform $\Delta x = 1/200$, and four singularity points were initially tracked: the shock and contact discontinuities arising at the left and at the right shock-tube configurations $\bar{S}_1$, C_1 and $\bar{S}_2$, C_2, respectively. Later, the $\bar{S}_1/\bar{S}_2$ shock interaction gives rise to two new shocks and a new contact discontinuity, which we denote $\bar{S}_3$, $\bar{S}_4$ and C_3. Still later, $\bar{S}_4$ interacts with C_2 giving rise to a transmitted shock $\bar{S}_5$ and a reflected rarefaction $\bar{R}_5$ (see Fig. 1b of [15]). All the singularities mentioned here were tracked (except $\bar{R}_5$ which was not treated as a singularity).

Our computational results are displayed at two points in time: at $t = 0.025$ (Fig. 3a) prior to any shock interaction, and at $t = 0.038$ (Fig. 3b) following a couple of shock interactions as explained above. Comparing our results (Fig. 3b) with those of PPMLR (Fig. 2h of [15]), we find a strong resemblance, except for the left part of $\bar{R}_5$, where our density distribution is monotonic while that of [15] exhibits a smooth peak. Repeating the computation with a two-fold refinement of the Eulerian grid

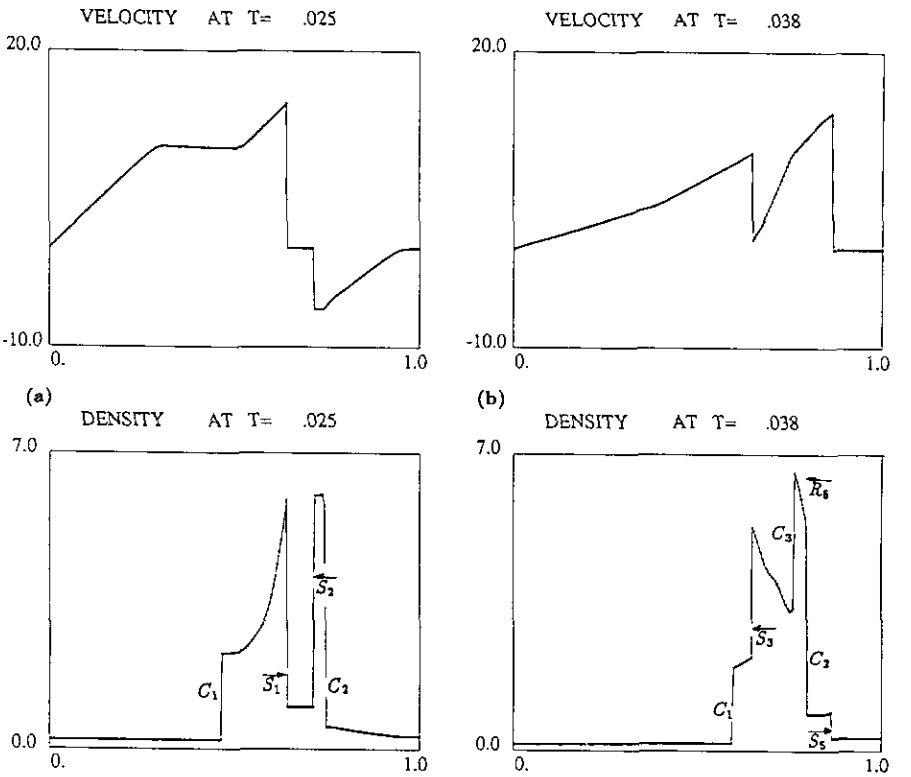

FIG. 3. Interacting blast waves: (a) at $t = 0.025$, prior to the shock interaction; (b) at $t = 0.038$, following a shock–shock interaction and the interaction of the right shock with the right-side contact discontinuity.

resulted in the same monotonic pattern of $\bar{R}_5$ as in Fig. 3b. This observation is also corroborated by a shock-tracking computation of the present test problem, performed by LeVeque & Shuye (see Fig. 13 of [8]).

Considering the mesh in our computation compared to that of [15], it is apparent that the GRP/ST scheme exhibits a significant gain in accuracy and resolution relative to untracked schemes. While the GRP/ST unified grid consisted of a Eulerian mesh having $\Delta x = 1/200$ augmented by (at most) seven singularity points, the PPMLR [15] computation employed a grid consisting of 3096 points, where the mesh size varied from $\Delta x = 1/2400$ to $\Delta x = 1/9600$, the finer mesh being assigned to the $\bar{R}_5$ region; moreover, the PPMLR computation resorted to an eight-fold mesh refinement in the vicinity of flow discontinuities.

(d) *Spherical Piston (Constant Velocity)*

Consider the flow generated by a spherical surface expanding at constant velocity U_p starting out from the origin into a sur-

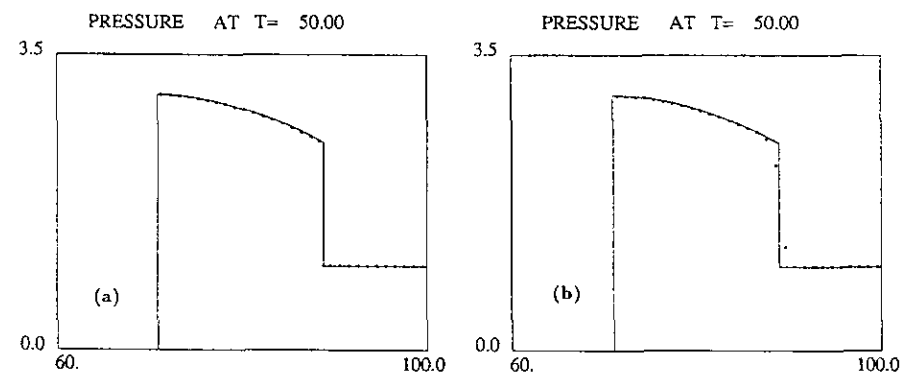

FIG. 4. Spherical piston expanding at constant speed: (a) at $t = 50$ with shock tracking, (b) at $t = 50$ without shock tracking.

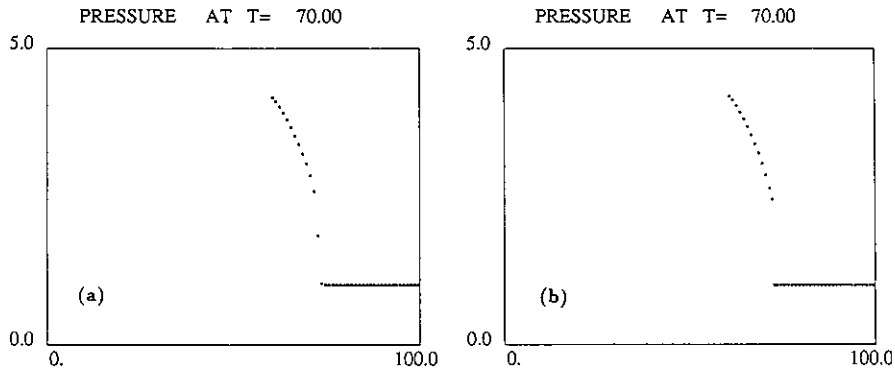

FIG. 5. Spherical piston expanding at constant acceleration: (a) at $t = 70$ without shock tracking; (b) at $t = 70$ with shock tracking.

rounding quiescent fluid. The shock Mach number was taken as $M_s = 1.5$ (the corresponding piston Mach number is about $M_p = 1.2$) and the fluid is assumed a perfect gas having $\gamma = 1.4$, $\rho_0 = 1$, and $p_0 = 1$. The computation domain ($0 < x < 100$) is divided into 100 equal cells. From the classical solution to this self-similar flow (Taylor [12]) we obtained the exact flow field by numerically integrating the pair of coupled ODE's; in Figs. 4a and 4b we compare the spatial pressure distribution between the piston and the shock for a tracked-shock computation and for an untracked one, with the exact solution. The accuracy of the tracked solution near the shock front is clearly superior to that of the untracked one.

(e) *Spherical Piston (Constant Acceleration)*

Consider the flow generated by a spherical surface expanding at constant acceleration $a_p = 0.02465$ starting out from the origin, into a quiescent perfect gas ($\gamma = 1.4$). The computation domain ($0 < x < 100$) is divided into 100 equal cells. Two computations were performed: one without shock tracking (Fig. 5a), the other (Fig. 5b) with tracking of the shock, using shock-trapping mechanism (see Section 4 in [6]). The results are shown at a time $t = 70$, where the shock is already well formed (note that the shock inception time for the corresponding planar piston is $t_c = 40$ [6]). Unlike a planar accelerated piston, the spherical one has no exact solution; hence the shock inception time can only be assessed from the computational results. When the trapping parameter was set to $\varepsilon_s = 0.05$ ($\varepsilon_s = (P_* - P_r)/\rho_r C_r^2$), the shock was trapped at $t = 55$, and when this value was set to $\varepsilon_s = 0.10$, the trapping moment moved up to $t = 59$. The results (in terms of $p(x)$ at $t = 70$) for either value of ε_s were virtually indistinguishable. It is concluded that while the moment of shock inception is not accurately determined by the trapping scheme, the post-formation shocked flow is insensitive to the precise numerical trapping moment. As to the comparison between the two types of computations, the shock resolution in the tracked computation (Fig. 5b) is clearly superior to that of the untracked computation (Fig. 5a).

REFERENCES

1. M. Ben-Artzi and J. Falcovitz, A second-order Godunov-type scheme for compressible fluid dynamics, *J. Comput. Phys.* **55,** 1 (1984).
2. M. Ben-Artzi and J. Falcovitz, An upwind second-order scheme for compressible duct flows, *SIAM J. Sci. Statist. Comp.* **7,** 744 (1986).
3. M. Ben-Artzi and A. Birman, Application of the generalized Riemann problem method for 1-D compressible flows with material interfaces, in *Proc. of the 15th International Symposium on Shock Waves, Berkeley, California, 1985,* edited by D. Bershader and R. Hanson (Stanford Univ. Press, Stanford, CA, 1985), p. 447.
4. M. Ben-Artzi and A. Birman, Application of the generalized Riemann problem method to 1-D compressible flows with material interfaces, *J. Comput. Phys.* **65,** 170 (1986).
5. J. Falcovitz and A. Birman, A singularities tracking conservation law scheme for compressible duct flows, in *Proc. of the 18th International Symposium on Shock Waves, Sendai, Japan, 1991,* edited by K. Takayama (Springer-Verlag, New York/Berlin, 1991), p. 1107.
6. J. Falcovitz and A. Birman, A singularities tracking conservation law scheme for compressible duct flows, TAE Report 717, Dept. of Aerospace Engineering, Technion, I. I. I. T., Haifa 32000, Israel, May 1994.
7. A. Harten and J. M. Hyman, Self adjusting grid methods for one-dimensional hyperbolic conservation laws, *J. Comput. Phys.* **50,** 235 (1983).
8. R. J. Le Veque and K. M. Shyue, Shock tracking based on high resolution wave propagation methods, Res. Rep. 92-01 SAM ETH, Zurich, Switzerland, 1992.
9. T. Saito and I. I. Glass, Application of random-choice method to problems in gas dynamics, *Prog. Aerospace Sci.* **21,** 201 (1984).
10. G. A. Sod, A survey of several finite difference methods for systems of non-linear hyperbolic conservation laws, *J. Comput. Phys.* **27,** 1 (1978).
11. B. K. Swartz and B. Wendroff, AZTEC: A Front Tracking Code Based on Godunov's method, *Appl. Numer. Math.* **2,** 385 (1986).
12. G. I. Taylor, The air wave surrounding an expanding sphere, *Proc. R. Soc. London A* **186** (1946).
13. B. van Leer, Towards the ultimate conservative difference scheme. II.

Monotonicity and conservation combined in a second-order scheme, *J. Comput. Phys.* **14,** 361 (1974).

14. B. van Leer, Towards the ultimate conservative difference scheme, V, *J. Comput. Phys.* **32,** 101 (1979).
15. P. R. Woodward and P. Colella, The numerical simulation of two-dimensional fluid flows with strong shocks, *J. Comput. Phys.* **54,** 115 (1984).
16. H. C. Yee, A class of high-resolution explicit and implicit shock-capturing methods, NASA Tech. Memo. 101088, Feb. 1989.